THE ASTROPHYSICAL JOURNAL, 270:758–768, 1983 July 15

THE EFFECT OF A NON-MAXWELLIAN ELECTRON DISTRIBUTION ON OXYGEN AND IRON IONIZATION BALANCES IN THE SOLAR CORONA

S. P. OWOCKI
High Altitude Observatory, National Center for Atmospheric Research[1]
AND
J. D. SCUDDER
NASA Goddard Spaceflight Center, Laboratory for Extraterrestrial Physics
Received 1982 October 18; accepted 1983 January 6

ABSTRACT

We derive analytic expressions for ionization and recombination rates in a parameterized non-Maxwellian electron velocity distribution with an enhanced high-energy tail. These expressions are then used to study the effect of such an enhancement in the high-energy tail of the coronal electron velocity distribution on the oxygen and iron ionization balances, $O^{+6} \leftrightarrow O^{+7}$ and $Fe^{+11} \leftrightarrow Fe^{+12}$. Relative to a Maxwellian of the same mean electron energy, we find the degree of ionization allowed by such a distribution is either unchanged or slightly decreased for iron, but is often substantially increased for oxygen. The greater sensitivity of oxygen ionization balance to the high-energy distribution tail results from the higher oxygen ionization threshold energy. Indeed, the electron temperature inferred from a measurement of the oxygen ionization ratio, O^{+6}/O^{+7}, could overestimate the actual coronal electron temperature by nearly 10^6 K if the coronal electron distribution is incorrectly assumed to be Maxwellian. The unexpectedly high degree of oxygen ionization inferred (e.g., from solar wind measurements of frozen-in ion flux ratios) for coronal source regions of high-speed solar wind may therefore result from an enhanced high-energy tail in the coronal electron velocity distribution, rather than from an enhanced coronal electron temperature.

We also discuss the general effect of the electron distribution shape, in addition to the electron temperature, on a plasma's ionization balance. As a general rule of thumb, we find the temperature T_m, inferred from a given ionization state measurement under the assumption that electron distribution is Maxwellian, is an overestimate (underestimate) of the actual temperature of a distribution with an enhanced high-energy tail if the inferred energy kT_m is less (greater) than half the ionization threshold energy $\chi/2$. We therefore conclude that the true character (i.e, temperature, shape) of the electron distribution function in a remote plasma like the solar corona is best inferred from local charge state information for several ionization balances with a range in ionization threshold energies.

Subject headings: atomic processes — Sun: corona

I. INTRODUCTION

The inferred degree of ionization in a remote astrophysical plasma is often used as a diagnostic of the plasma electron temperature. In particular, in the solar corona, where photoionization can be neglected (Billings 1966), the equilibrium ionization balance is fixed by the competition between ion-electron collisional ionization (both direct and via autoionizing levels; Seaton 1964; Lotz 1967) and dielectronic and/or radiative recombination (Burgess 1965; Jacobs *et al.* 1977). If the electron velocity distribution is Maxwellian, then ionization can be increased relative to recombination only by increasing the mean electron energy, and so the degree of ionization in this case is a reasonable electron temperature diagnostic (see, e.g., Allen and Dupree 1969; Jordan 1969). If the distribution is *not* Maxwellian, then the ratio of ionization to recombination can also be changed by altering the distribution shape, and so the degree of ionization in this case is no longer a simple temperature diagnostic. Motivated by the expectation that the electron velocity distribution in many astrophysical plasmas may not be Maxwellian (Scudder and Olbert 1983; see below), we shall examine in this paper the effect of the electron distribution shape on a plasma's ionization balance. As a specific example, we shall examine in detail the effect of a non-Maxwellian coronal electron distribution on the ionization balances among the dominant charge stages of the coronally-abundant heavy elements oxygen and iron, i.e., $O^{+6} \leftrightarrow O^{+7}$ and $Fe^{+11} \leftrightarrow Fe^{+12}$.

[1]The National Center for Atmospheric Research is sponsored by the National Science Foundation.

There exists both observational and theoretical evidence that the electron velocity distributions in many astrophysical plasmas are not Maxwellian. For example, direct measurements have shown the electron distributions to be non-Maxwellian in the magnetospheres of Mercury (Ogilvie *et al.* 1974, 1977), Venus (Bridge *et al.* 1974), Earth (Vasyliunas 1968; Garrett 1979; Krimigis *et al.* 1981), Jupiter (Belcher, Goertz, and Bridge 1980; Krimigis *et al.* 1981; Scudder, Sittler, and Bridge 1981), and Saturn (Sittler, Scudder, and Bridge 1981). In addition, remote observations of radio spectra have provided indirect evidence for non-Maxwellian electron distributions in radio sources both within (e.g., solar flares: Smerd 1964) and external to our solar system (see, e.g., Kraus 1966). Furthermore, inferences, based on remote ultraviolet spectral observations (Strobel and Davis 1980), that the electron distribution in Io's plasma torus is not Maxwellian have been subsequently confirmed by direct measurements (Scudder, Sittler, and Bridge 1981). Finally, direct measurements have also shown that, while the low-energy "cores" of the electron velocity distributions in the solar wind can be well fitted by a Maxwellian, the high-energy "tails" of these distributions are best fit by a power law, and so are enhanced relative to a Maxwellian of the same mean particle energy (Montgomery, Bame, and Hundhausen 1968; Montgomery 1972; Feldman *et al.* 1975; Rosenbauer *et al.* 1976; Ogilvie and Scudder 1978).

Scudder and Olbert (1979*a*, *b*) have argued that the observed enhancement in the high-energy tail of the interplanetary electron velocity distribution arises because of the decline of the Coulomb collision cross section at high electron energies. This allows higher energy coronal electrons to travel with few collisions upward from the high-density corona into the low-density solar wind, where they enhance the tail of the local distribution. According to this theory of global transport for high-energy electrons, the strong density gradient throughout the solar corona should also result in locally enhanced high-energy tails in the electron velocity distribution of the corona itself (Scudder and Olbert 1982). Similarly, Roussel-Dupré (1979, 1980*a*) and Shoub (1983) have argued that coronal electrons, with their high mean energy, can collisionlessly propagate *downward* and thereby enhance the high-energy tail of the loca electron distribution in the chromosphere-corona transition region, where the mean energy is much lower. In general, these theoretical arguments suggest that enhancements in the high-energy electron distribution tail arise naturally in fully ionized plasmas with strong gradients in density (e.g., solar corona and solar wind) or temperature (e.g., solar transition region), and so non-Maxwellian distributions should exist in many astrophysical plasmas, where such conditions are common.

In this paper, we shall examine how such an enhanced high-energy tail can affect the degree of ionization in such plasmas. Whereas previous studies have examined this question only for non-Maxwellian distributions calculated from detailed models for specific plasmas (e.g., for the solar transition region; Roussel-Dupré 1980*b*; Shoub 1983), we shall employ here (see Appendix A) a parameterized form, the "kappa distribution" (Olbert *et al.* 1967; Olbert 1969) for which the relative deviation of the distribution from a Maxwellian shape can be readily varied through changes in the free parameter, κ. As with the distributions observed in the solar wind and postulated for the solar corona and transition region, this kappa distribution closely approximates a Maxwellian in the low-energy "core," but varies as a power law in its enhanced high-energy tail. Using general analytic expressions for ionization and recombination rates (derived in Appendix B) in this parameterized non-Maxwellian distribution, we shall study how the degree of ionization in a plasma depends in general on the shape of the electron distribution (i.e., on the magnitude of the high-energy tail enhancement), as well as on the electron temperature.

In particular, to illustrate general effects more concretely, we shall examine in detail the influence of the distribution shape on the specific ionization balances, $O^{+6} \leftrightarrow O^{+7}$ and $Fe^{+11} \leftrightarrow Fe^{+12}$, which represent the exchanges among the dominant charge stages of these abundant heavy elements in the solar corona. We shall show quantitatively how differences in the ionization potentials for these two exchanges result in marked differences in how they are affected by an enhanced high-energy tail in the electron distribution. We shall then generalize this result to derive a simple rule of thumb that describes how the presence of an enhanced high-energy tail alters the use of information on a plasma's ionization state as a diagnostic of the electron temperature. Finally, we shall apply these results to the interpretation of certain observational inferences on the degree of ionization of oxygen and iron in the solar corona.

II. THE IONIZATION STATE AS AN ELECTRON TEMPERATURE DIAGNOSTIC

In the absence of intrinsic or advective time variations, the ionization state of a parcel of gas approaches a steady-state equilibrium in which the number density n_i of ions in the ionization stage i of a given species is fixed by competition between ionization and recombination into and out of i, and so

$$\frac{n_i}{n_{i+1}} = \frac{R_{i+1}}{C_i}, \tag{1}$$

where R_{i+1} and C_i are the recombination and ionization rates from the appropriate stages $i+1$ and i. If we assume the ambient radiation field is weak, then photo-

ionization can be neglected, and ionization (both direct and via autoionizing states; Seaton 1964; Lotz 1967) occurs by ion-electron collisions that compete with dielectronic and radiative recombination (Burgess 1965; Jacobs *et al.* 1977). (We also assume here that the electron density n_e is low enough that all three-body processes can be neglected.) Such an ionization balance is often referred to as coronal ionization equilibrium, although it holds in any low-density plasma with a weak radiation field.

Under these circumstances, each of the rates R and C can be written in the form $n_e\langle\sigma v\rangle$, where v is the electron speed, σ is a density-independent cross section for the process (see Appendix B), and the angular brackets denote an average over the electron velocity distribution f. The electron velocity distribution function $f(\boldsymbol{r}, \boldsymbol{v})$ at a location $\boldsymbol{r}$ describes the probability $f(\boldsymbol{r}, \boldsymbol{v})\, d\boldsymbol{v}$ that an electron occupies a volume element $d\boldsymbol{v}$ in velocity space centered on the velocity $\boldsymbol{v}$. Here we assume an isotropic[2] velocity distribution $f(\boldsymbol{r}, \boldsymbol{v}) = f(\boldsymbol{r}, v)$ so that the rates can be written as an average in electron kinetic energy, $E \equiv mv^2/2$,

$$\langle \sigma v \rangle = \frac{8\pi}{m^2} \int_0^\infty \sigma f E \, dE, \tag{2}$$

where m is the electron mass. Analytic approximations to each cross section and the resulting rates for specific forms of the electron distribution are given in Appendix B.

Because each of the rates R and C is proportional to electron density, the rate ratio R/C is clearly independent of density, and so the equilibrium ionization ratio, n_i/n_{i+1}, between neighboring charge stages depends only on the ratios of the rate coefficients, $\langle \sigma_R v \rangle / \langle \sigma_C v \rangle$ (eq. [1]). Whereas recombination occurs preferentially with low-energy electrons, ionizations can occur only through ion collisions with electrons that have kinetic energy above a given ionization threshold. In a Maxwellian distribution (Appendix A), the ionization rate therefore increases relative to the recombination rate as the fraction of electrons with energies above the ionization threshold energy χ increases with an increasing mean energy, and so the equilibrium ionization ratio (1) decreases to favor ionization as the electron temperature is increased. It is through this temperature dependence that information on ionization state has been traditionally used to infer remotely the electron temperature, with the *assumption* that the electron velocity distribution is well described by a Maxwellian shape. Given the evidence presented above (see § I) that electron distributions are often markedly non-Maxwellian in many low-density astrophysical plasmas, we shall now investigate how a non-Maxwellian shape of the electron distribution can affect ionization and recombination rates, and so can modify the use of information on a plasma's ionization state as a diagnostic of the electron temperature.

[2] In the presence of a magnetic field or gradients in bulk quantities, the distribution f will be anisotropic, and so the rate integrals (2) may depend on angle as well as energy; but the leading order effects we investigate here arise from the energy dependence of f and σ, and so the simplifying assumption of isotropy is not very restrictive.

III. IONIZATION AND RECOMBINATION RATES IN NON-MAXWELLIAN DISTRIBUTIONS

In order to study the effect of a non-Maxwellian electron distribution on a plasma's ionization balance, we define in Appendix A a parameterized function, the "kappa distribution" (Olbert *et al.* 1967; Olbert 1969) that economically simulates the shapes of observed and postulated distributions with Maxwellian low-energy cores and power-law high-energy tails. The added freedom to specify the shape of a kappa distribution, in addition to its mean energy $\langle E \rangle$ ($= 3kT/2$, where T is the temperature), is reflected in the free parameter κ, which controls the prominence of the non-Maxwellian high-energy tail. A convenient way to characterize physically the degree to which a kappa distribution can be approximated by a Maxwellian is by the quantity $E_p/kT = (\kappa - 3/2)/\kappa$, the ratio of core energy to total energy (see Appendix A). Figure 1 compares kappa distributions that have either strong ($\kappa = 2$; $E_p/kT = 0.25$) or moderate ($\kappa = 5$; $E_p/kT = 0.70$) non-Maxwellian character with a Maxwellian ($\kappa = \infty$; $E_p/kT = 1$) of equal temperature T. Note that the high-energy tails ($E \gg kT$) of the kappa distributions are enhanced relative to the Maxwellian, but, because of the simultaneous requirements of overall density normalization and equal temperature (i.e., equal mean energy) for all distributions, the kappa distributions are also enhanced at low-energies ($E \lesssim kT$), and depleted at intermediate energies ($kT < E < 4kT$). These enhancements or depletions lead to ionization or recombination rate increases or decreases according to which portion of the distribution controls the rate integrals (2).

Appendix B gives analytic forms for ionization and recombination cross sections and for the associated rates calculated from equation (2) for both the Maxwellian and kappa distributions. In Figure 2 the ratio $\beta_c \equiv \langle \sigma_c v \rangle_\kappa / \langle \sigma_c v \rangle_{\max}|_{T=\text{const}}$ (cf. eqs. [B2a] and [B3a]) of the direct collisional ionization rate in a kappa distribution over that in a Maxwellian with the same temperature T is plotted versus χ/kT, the ratio of ionization energy to thermal energy. Because of the enhancement in the high-energy tail of the kappa distribution, the kappa ionization rate is greatly increased when the ionization threshold energy χ is large relative to the thermal energy kT (i.e., $\beta_c \gg 1$ when $\chi/kT \gg 1$); but, because of the depletion of the kappa distribution at intermediate energies, there can also be kappa ionization rate reductions

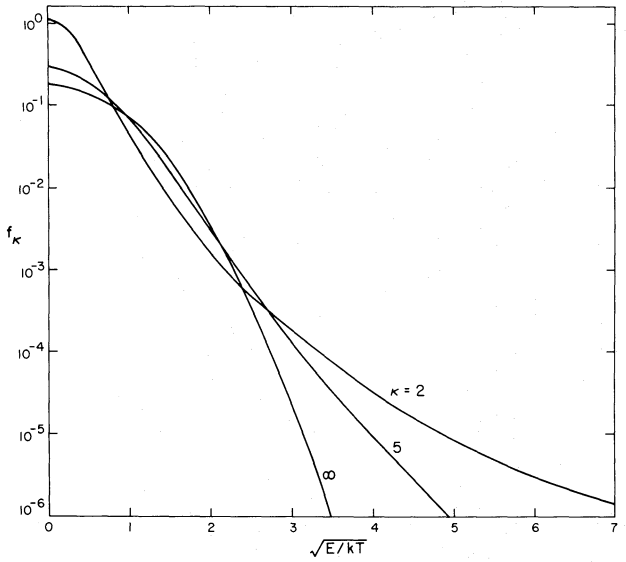

FIG. 1.—Kappa electron distribution function f_κ (in units of $(2kT/m)^{-3/2}$) vs. the square root of the electron kinetic energy over thermal energy, $(E/kT)^{1/2}$, for kappa distributions with $\kappa = 2$ and 5 (energy ratios $E_p/kT = 0.25$ and 0.70), and a Maxwellian ($\kappa = \infty$; $E_p/kT = 1$). The temperature T is assumed to be equal for all three distributions.

for moderate ionization energies (i.e., $\beta_c < 1$ when $\chi/kT \lesssim 1$). The effects on autoionization rates are qualitatively similar to these for direct collisional ionization (cf. eqs. [B2b] and [B3b]).

In contrast to ionization, radiative recombination can occur with electrons of energy *below* ionization threshold, and, in fact, is more likely for these low-energy electrons (see eq. [B1c]). Comparison of equations (B2c) and (B3c) shows:

$$\beta_r \equiv \left[\frac{\langle \sigma_r v \rangle_\kappa}{\langle \sigma_r v \rangle_{\max}}\right]_{T=\text{const.}} = \frac{\Gamma(\kappa + a - 1)}{\Gamma(\kappa - 1/2)(\kappa - 3/2)^{a-1/2}}, \quad (3)$$

where the energy exponent a (see eq. [B1c]) is typically between 1/2 and 1. For $a = 1/2$, we find $\beta_r = 1$ for all values of κ, and, for $a = 1$, we still obtain $\beta_r \lesssim 1.5$ for $\kappa \geq 2$. Thus radiative recombination in a kappa distribution occurs at or slightly above the rate in the analogous Maxwellian.

Dielectronic recombination occurs with electrons with discrete energies E_{di} below the ionization threshold energy χ. If $kT \ll E_{di} \lesssim \chi$, then a kappa distribution will have many more electrons at the resonance energies than a Maxwellian, and the kappa dielectronic recombination rate can, in principle, be enhanced. In practice, such enhancements are rarely important, as can be seen by assuming, for simplicity, that the resonance at a single energy E_0 dominates. The ratio of dielectronic rates can then be written

$$\beta_d \equiv \left[\frac{\langle \sigma_d v \rangle_\kappa}{\langle \sigma_d v \rangle_{\max}}\right]_{T=\text{const.}} \approx \left\{\exp(E_0/kT) \Big/ \left[1 + \frac{1}{\kappa - 3/2}\frac{E_0}{kT}\right]^{\kappa+1}\right\} \times \frac{\Gamma(\kappa+1)}{\Gamma(\kappa - 1/2)(\kappa - 3/2)^{3/2}}. \quad (4)$$

For the extreme non-Maxwellian case $\kappa = 2$, we find $\beta_d \lesssim 2$ as long as $0.3 \lesssim E_0/kT \lesssim 8$, an assumption that is not very restrictive for balances among abundant ionization stages.

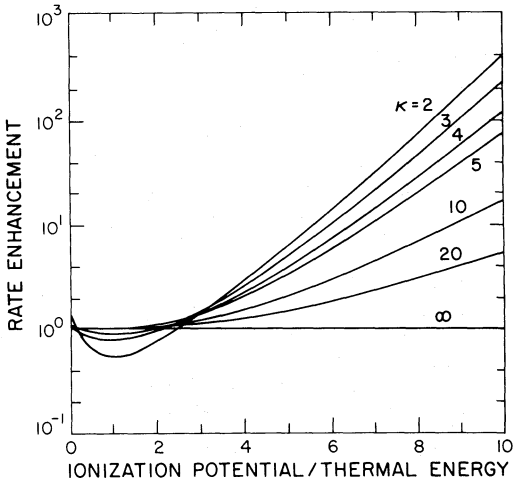

FIG. 2.—Ionization rate enhancement of a kappa distribution relative to a Maxwellian with the same temperature T, as a function of χ/kT, the ratio of the ionization threshold energy to electron thermal energy.

IV. EFFECT OF NON-MAXWELLIAN DISTRIBUTIONS ON CORONAL IONIZATION BALANCES

Motivated by the expectation that the coronal electron velocity distribution may be non-Maxwellian (Scudder and Olbert 1982), and by solar wind measurements showing an unexpectedly high frozen-in oxygen ionization state (Ogilvie and Vogt 1980), we consider in detail the effect of non-Maxwellian electron distributions on the coronal ionization exchanges, $O^{+6} \leftrightarrow O^{+7}$ and $Fe^{+11} \leftrightarrow Fe^{+12}$. Although the lower level of each of these exchanges is the most abundant stage in an equilibrium balance at a typical coronal temperature of 1.5×10^6 K (Allen and Dupree 1969; Jordan 1969, 1970), the oxygen ionization threshold energy is actually more than twice that of iron [i.e., $\chi(O^{+6}) = 739$ eV vs.

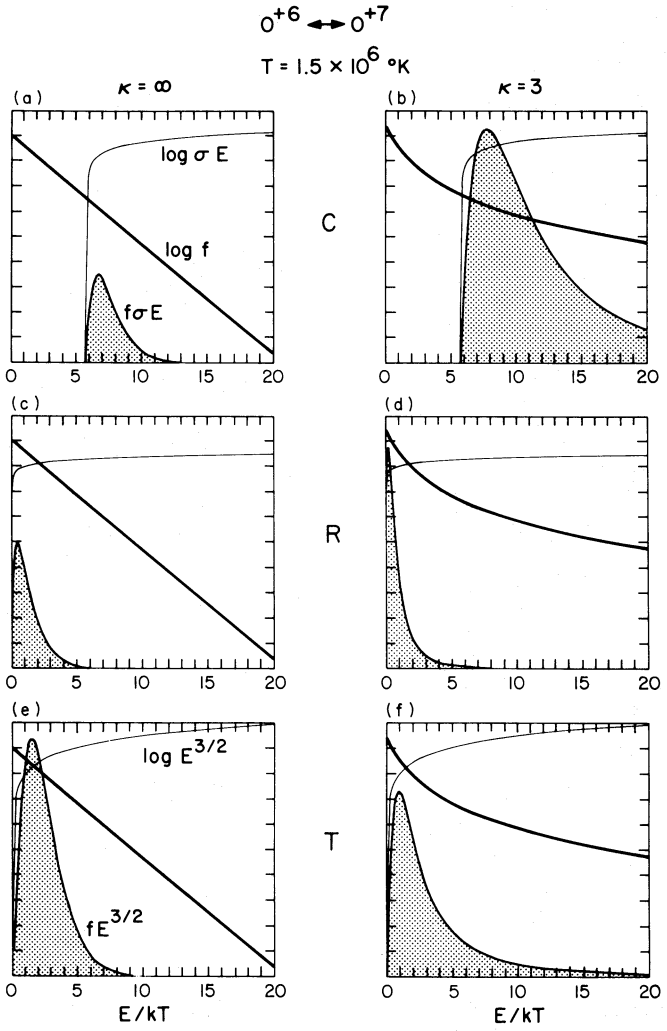

FIG. 3.—Comparison of collisional ionization (C) and radiative recombination (R) for the oxygen ionization balance $O^{+6} \leftrightarrow O^{+7}$ in a Maxwellian ($\kappa = \infty$; *left boxes*) and in a kappa distribution ($\kappa = 3$; *right boxes*). In the upper four boxes (a)–(d), the heavy and light solid lines show, respectively, the logarithmic variations of the distribution function f and the cross section times energy σE, while the linear variation of the relevant rate integrand $f\sigma E$ outlines the shaded areas, which are thus proportional to the relevant rates $\langle \sigma v \rangle$. In the lower two boxes (e)–(f), the cross section is replaced by the square root of the energy, $E^{1/2}$, and the equality of the shaded areas, now proportional to the mean kinetic energy $\langle E \rangle = 3kT/2$, shows that the two distributions have the same kinetic temperature ($T = 1.5 \times 10^6$ K). Likewise, the near equality of the areas in the central two boxes (c)–(d) shows that the radiative recombination rate is nearly equal in the two distributions, while the much greater shaded area for (b) as compared to (a) shows that the collisional ionization rate is greatly enhanced in the kappa distribution.

$\chi(Fe^{+11}) = 331$ eV]. An enhanced high-energy tail in the coronal electron distribution would therefore be more likely to increase the local degree of oxygen ionization.

Figure 3 graphically illustrates for the oxygen ionization exchange $O^{+6} \leftrightarrow O^{+7}$ the relative sensitivity of collisional ionization rate and radiative recombination rate to the presence of an enhanced tail on the electron distribution function. In each of the upper, central, and lower two boxes of Figure 3, the shaded areas are proportional respectively to the ionization rate, recombination rate, and mean electron energy (i.e. electron temperature) in either a Maxwellian distribution (i.e., with $\kappa = \infty$; *left boxes*) or in a kappa distribution with $\kappa = 3$ (*right boxes*). The two distributions have been adjusted to have equal temperatures $T = 1.5 \times 10^6$ K, as can be seen from the equality of the shaded areas in the lower two boxes (cf. Figs. 3*e*, *f*). Comparison of the shaded areas in the central two boxes (cf. Figs. 3*c*, *d*), which are proportional to the respective radiative recombination rates, shows that in the kappa distribution recombination occurs at a slightly higher rate, and with electrons of slightly lower energy, than in the Maxwellian. By contrast, the impact ionization rates are significantly increased by the enhanced high-energy tail of the kappa distribution (cf. Figs. 3*a* and 3*b*). The net result (see eq. [1]) is that a kappa distribution can support a

much higher degree of oxygen ionization than a Maxwellian with the same temperature. Qualitatively, we therefore expect that interpretations of the oxygen charge state based on the assumption of a Maxwellian will systematically overestimate the electron temperature if the electron distribution actually has an enhanced high-energy component.

Because it is the ionization ratio, n_i/n_{i+1} ($= R_{i+1}/C_i$ in ionization equilibrium; eq. [1]), and not the individual rates R_i or C_i, that can be observed (either spectroscopically or by direct sampling), it is important to establish quantitatively the range in electron distribution function properties that are compatible with a given ratio in ionization equilibrium. In Figures 4*a* and 4*b* contours of the iron (Fe^{+11}/Fe^{+12}) and oxygen (O^{+6}/O^{+7}) equilibrium ionization ratios are plotted for electron velocity distributions that range from Maxwellian ($\kappa = \infty$; $E_p/kT = 1$) to extremely non-Maxwellian ($\kappa = 2$; $E_p/kT = 0.25$), and that range in temperature from $T = 1 \times 10^6$ K to 3×10^6 K. The path along any contour denotes the appropriate combinations of T and E_p/kT that are consistent with an ionization ratio measurement of the value that labels the contour. For example, note from Figure 4*b* that an oxygen ionization ratio $n_{+6}/n_{+7} = 1$ is consistent with a Maxwellian distribution with $T \approx 2 \times 10^6$ K and $E_p/kT = 1$, but it is also consistent with a kappa distribution with $T \approx 1.3 \times 10^6$ K and $E_p/kT \approx 0.4$ (i.e., $\kappa \approx 2.5$). If the latter parameter set better represented the electron distribution function in a remote astrophysical plasma, then an oxygen ionization ratio measurement, if interpreted on the basis of the traditional assumption of a Maxwellian electron distribution, would lead to an electron temperature overestimate of about 0.7×10^6 K.

V. DISCUSSION

A temperature overestimate of this kind will occur whenever the contours in Figure 4 slope downward as one moves away from Maxwellian limit denoted by the left ordinate. Conversely, an upward slope implies a temperature underestimate when one incorrectly assumes a Maxwellian, while a zero (or small) slope implies that the equilibrium ionization ratio is relatively insensitive to assumptions about the form of the distribution. The oxygen contours generally slope downward; the iron contours either have zero or upward slopes (cf. Figs. 4*a* and 4*b*). Hence, in contrast to the temperature overestimates typical for oxygen, the iron charge state ratios either are insensitive to the form of the distribution or yield temperature underestimates when a Maxwellian is incorrectly assumed (viz., the contour labeled "1" in Fig. 4*a*). Even the oxygen contours do not, however, continue to slope downward for extreme departures from a Maxwellian; rather they reach a minimum for $E_p/kT \approx 0.4$–0.5, so that the magnitude of temperature overestimates based on measured oxygen ionization ratios is limited to $\lesssim 0.75 \times 10^6$ K. This up-

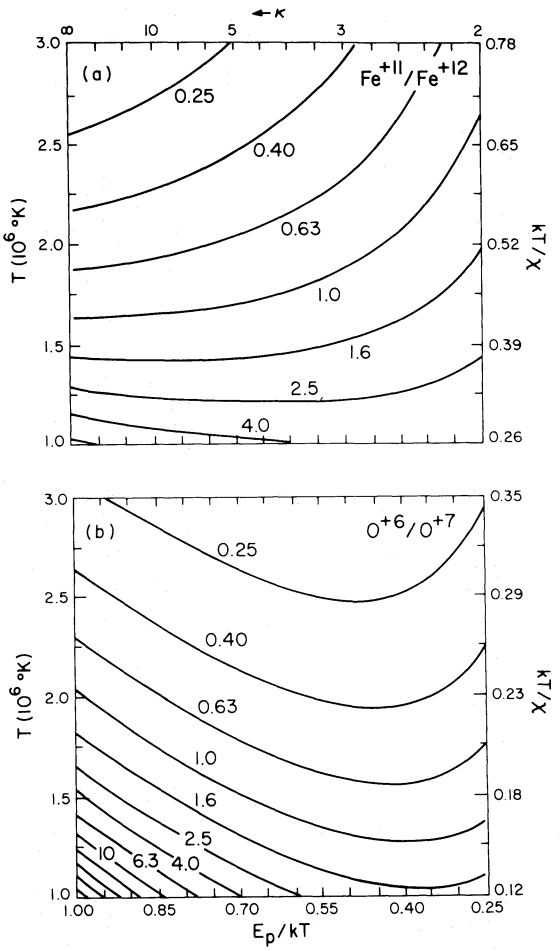

FIG. 4.—(*a*) Contours of iron ionization ratio Fe^{+11}/Fe^{+12} as a function of kinetic temperature T and of core to total energy ratio E_p/kT. The right ordinate is labeled with the ratio, kT/χ, of thermal energy to ionization threshold energy; the upper abscissa is labeled with the value of the distribution parameter κ; and each contour is labeled with the appropriate ionization ratio. (*b*) Same as Fig. 4*a*, except for the oxygen ratio O^{+6}/O^{+7}.

turn in equilibrium ionization ratio contours for extreme non-Maxwellian distributions stems mostly from the recombination rate increase associated with the enhancement in the low-energy energy core of the distribution (see Fig. 1, also Figs. 3*c* and 3*d*).

For milder deviations from a Maxwellian, the recombination rate is relatively insensitive to changes in the shape of the distribution (see § III), and so the slopes of ratio contours in Figures 4 as one moves away from the Maxwellian limit ($E_p/kT = 1$) primarily reflect the properties of just the ionization rate. This is illustrated by Figure 5, in which contours of the generic ionization rate (eq. [B3a]) are plotted as functions of kT/χ, the ratio of electron energy over ionization threshold energy, and of the energy ratio E_p/kT. Moving from the Maxwellian limit $E_p/kT = 1$, the rate contours in Figure 5 slope downward (upward) when the ratio kT/χ is less

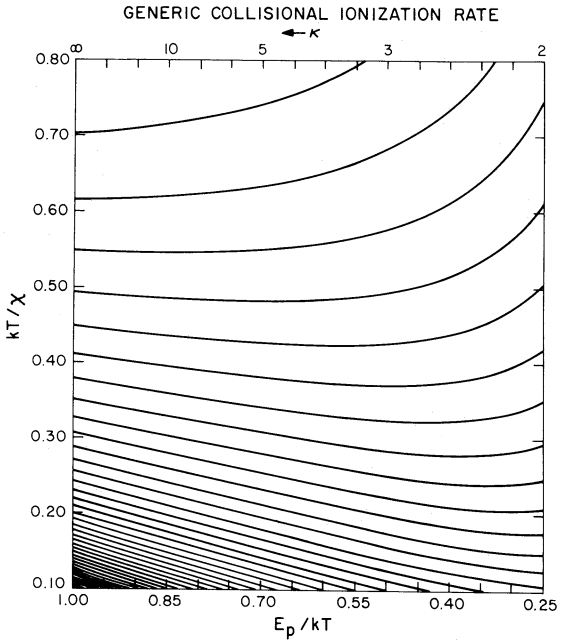

FIG. 5.—Contours of a generic ionization rate integral, spaced logarithmically at 10 contours per decade, as functions of the core to total energy ratio, E_p/kT, and of kT/χ, the ratio of thermal energy to ionization threshold energy.

(greater) than one-half. The upward-sloping regime is appropriate for the iron ionization exchange $Fe^{+11} \leftrightarrow Fe^{+12}$ (cf. Fig. 4*a*), while the downward slope characterizes the oxygen exchange $O^{+6} \leftrightarrow O^{+7}$ (cf. Fig. 4*b*). The dimensionless energy ratio $kT/\chi \approx 1/2$ thus roughly separates the regimes for errors in ionization diagnostics of the electron temperature, and we can formulate the following simple rule of thumb: If, for a given ionization ratio measurement, the temperature T_m, inferred by assuming a Maxwellian distribution, is such that $T_m < \chi/2k$ ($T_m > \chi/2k$), then this is likely to be an overestimate (underestimate) of the correct electron kinetic temperature T if the distribution is actually non-Maxwellian with an enhanced high-energy tail. The possibility that ionization state measurements could lead to *underestimates* of the temperature of such a distribution was not obvious before this study, but it now can be easily seen to arise from the decrease in the ionization rate when the ionization threshold lies at intermediate energies, at which these non-Maxwellian distributions are depleted relative to a Maxwellian of the same temperature (Fig. 1).

If information on the degree of ionization of both oxygen and iron were available for the same local coronal volume, a comparison could yield constraints on the form of the coronal electron distribution. For example, assuming the distribution can be approximated by a kappa function (i.e., that it has a Maxwellian low-energy core and a power-law high-energy tail), the intersection of appropriate contours, plotted from Figures 4*a* and 4*b* for the measured oxygen and iron ionization ratios, would yield both the temperature of the distribution and its deviation from a Maxwellian. Unfortunately, the coronal ionization state cannot be measured directly, but must be inferred remotely—e.g., from solar wind measurements of ionization ratios that freeze at various heights in the corona (Hundhausen, Gilbert, and Bame 1968*a*, *b*), or from observation of optically thin spectral line emission integrated along the line of sight (Billings 1966). In either case, both a temperature gradient and a locally non-Maxwellian distribution have similar effects on the observables, and so the interpretation of these observations is ambiguous. This ambiguity can, however, be reduced for spectral observations by combining information from several lines of sight (e.g., as is done to infer coronal electron density from white light observations of the corona; Wilson 1977), and so spatially resolved observation of coronal spectral lines from many ion stages with a range in ionization thresholds could yield constraints on the form of the coronal electron distribution.

In the solar wind the electron velocity distribution is directly measured to be distinctly non-Maxwellian (e.g., Montgomery, Bame, and Hundhausen 1968; Montgomery 1972; Feldman *et al.* 1975), but this has little effect on local ionization balances because the solar wind ionization state is "frozen" in the corona by expansion effects (Hundhausen, Gilbert, and Bame 1968*a*, *b*). In fact, by assuming that the electron velocity distribution is Maxwellian in the coronal freezing-in region, interplanetary charge states (e.g., of oxygen and iron), inferred from measurements of solar wind ion flux versus mass-per-charge, have traditionally been used to estimate the electron temperature in the coronal source regions of the solar wind. The inferred interplanetary oxygen ionization state typically implies coronal freezing-in temperatures from 1.5×10^6 K to 3×10^6 K that are positively correlated with the wind speed (Ogilvie and Vogt 1980). Freezing-in temperatures ($\sim 1.5\times10^6$ K) derived from measurements of the solar-wind charge state of iron are generally lower than those derived from oxygen (Bame *et al.* 1974; Fenimore 1980). Because iron typically freezes higher in the expansion than oxygen, this difference may simply reflect a decline in the electron temperature with height, but it is also qualitatively consistent with the relative behavior of the oxygen and iron ionization states in the presence of an enhanced tail on the electron velocity distribution.

For the high-speed solar wind, the coronal temperatures inferred from the frozen-in oxygen charge state ($\sim 3\times10^6$ K; Ogilvie and Vogt 1980) are substantially higher than upper limits on the base electron temperature ($T_e \lesssim 2\times10^6$ K) derived from simultaneous consideration of the coronal dynamical implications of both the observed base pressure and the measured solar wind

mass flux at 1 AU (Leer and Holzer 1979). Both this discrepancy and the correlation of freezing-in temperature with wind speed could be explained by postulating that enhanced tails in the electron velocity distribution are more pronounced in the coronal source regions of high-speed solar wind than in sources of low-speed wind. Because enhanced tails are associated with gradients in bulk properties (Scudder and Olbert 1983), such a postulate would be consistent with the expectation that the electron density gradient is strongest in the rapidly diverging flow geometries (i.e., coronal holes; Munro and Jackson 1977) that characterize the coronal source regions of the highest-speed solar wind.

Recall, however, from § IV that the magnitude of the non-Maxwellian enhancement in the inferred oxygen ionization temperature enhancement is limited to $\lesssim 10^6$ K. This limitation is not unique to the specific parameterized distribution function for which it was derived (see Owocki 1982); rather it arises from the intrinsic difficulty of increasing the degree of ionization by enhancing the high-energy tail of an electron distribution function—i.e., at energies slightly above the ionization threshold—without also increasing the electron temperature. We therefore conclude that occasional very high inferred oxygen freezing-in temperatures $\gtrsim 3\times 10^6$ K (Ogilvie and Vogt 1980) cannot be totally explained by postulating that the coronal electron velocity distribution is non-Maxwellian.

Finally, we note that, in general, marked deviations from a Maxwellian distribution should be common in low-density astrophysical plasmas, for which gradients in either density or temperature are ubiquitous. Because ions with different ionization threshold energies respond differently to a non-Maxwellian shape in the electron velocity distribution, the proper interpretation of the overall ionization state inferred for these plasmas therefore should take into account the possible effects of a non-Maxwellian distribution. In particular, the very strong temperature gradients expected in solar and stellar transition regions imply that electrons propagating from hotter to cooler levels will skew the local distribution function from a Maxwellian shape, and so the transition region ionization state (e.g., as inferred from observations of ultraviolet spectral lines) cannot be naively interpreted in terms of the local electron temperature (Roussel-Dupré 1979, 1980*a*, *b*; Shoub 1983). Likewise, because gradients in density and temperature are likely in the outer atmospheres and winds of late type stars (in addition to the Sun), the effects of a non-Maxwellian electron velocity distribution may also be important for interpreting spectral features formed in these environments.

VI. SUMMARY

In this paper, we have used a parameterized electron velocity distribution function to investigate the effects of an enhanced high-energy distribution tail on the collisional ionization balance of a plasma. We have found that the recombination rate in such a distribution differs only slightly from that in a Maxwellian with the same mean electron energy (i.e., same temperature T), while the ionization rate can be substantially greater if the ionization threshold energy χ is large compared to the thermal energy kT. This means that the degree of ionization in a plasma depends on the shape of the electron distribution, as well as on the electron temperature. Conversely, the inverse problem of accurately estimating the electron temperature of a remote plasma from its inferred ionization state data contains an intrinsic ambiguity that heretofore has been largely ignored.

Motivated by the expectation that the electron velocity distribution in the solar corona may have an enhanced high-energy tail, we have specifically investigated the effects of non-Maxwellian electron distribution on the oxygen and iron ionization balances, $O^{+6} \leftrightarrow O^{+7}$ and $Fe^{+11} \leftrightarrow Fe^{+12}$. We found that, because of high ionization energy for O^{+6}, interpretations of the oxygen ionization state based on the assumption of a Maxwellian can overestimate by as much as 0.8×10^6 K the true electron temperature of a distribution with an enhanced high-energy tail. This effect could explain the very high coronal electron temperature inferred from analysis of measurements of the frozen-in oxygen charge state in the solar wind. We also found that, because of its lower ionization energy, Maxwellian-based interpretations of the iron ionization state mildly underestimate the actual temperature of such non-Maxwellian distributions. Finally, as a general rule of thumb, we found that the temperature T_m, inferred from a given ionization state measurement under the assumption that electron distribution is Maxwellian, is an overestimate (underestimate) of the actual temperature of a distribution with an enhanced high-energy tail if the inferred thermal energy kT_m is less (greater) than half the ionization threshold energy $\chi/2$. We therefore conclude that the true nature of the electron distribution in a remote plasma like the corona is best probed with measurements from the same spatial location of the relative abundances of many ion charge stages with a variety of ionization threshold energies.

We wish to thank S. Migliuolo, T. Holzer, G. Withbroe, and J. Raymond for their useful comments on various versions of this manuscript. The results reported here are based on thesis research done with support of a graduate research assistantship at the High Altitude Observatory of the National Center for Atmospheric Research. This paper was prepared with support of the Langley-Abbott program of the Smithsonian Institution and NASA grant NAGW-249.

APPENDIX A

THE ELECTRON VELOCITY DISTRIBUTION FUNCTION

The electron velocity distribution function $f(\boldsymbol{r}, \boldsymbol{v})$ describes the probability $f(\boldsymbol{r}, \boldsymbol{v})\, d\boldsymbol{v}$ that an electron at spatial location $\boldsymbol{r}$ occupies a volume element $d\boldsymbol{v}$ in velocity space centered on the velocity $\boldsymbol{v}$. In an isotropic, homogeneous plasma isolated from external influences, the distribution depends only on the electron kinetic energy $E = mv^2/2$ in the center-of-mass coordinate system, and approaches the Maxwellian form,

$$f_{\max}(E) = \left(\frac{m}{2\pi kT}\right)^{3/2} e^{-E/kT}, \tag{A1}$$

where m is the electron mass, k is Boltzmann's constant, and the temperature T characterizes the mean particle energy $\langle E \rangle = 3kT/2$.

Although it is common practice in astrophysics to assume a Maxwellian distribution, the strong inhomogeneity of many astrophysical plasmas often results in a distribution with an enhanced high-energy tail (see § I). A parameterized function that conveniently simulates this non-Maxwellian property is given by the "kappa distribution" (Olbert *et al.* 1967; Olbert 1969)

$$f_\kappa(E) = \left(\frac{m}{2\pi kT}\right)^{3/2} A_\kappa \Big/ \left(1 + \frac{E}{(\kappa - 3/2)kT}\right)^{\kappa+1}, \tag{A2}$$

where the temperature T again characterizes the mean energy $\langle E \rangle$, $\Gamma(\kappa + 1) \equiv \kappa!$ is the gamma (generalized factorial) function (Abramowitz and Stegun 1972), and $A_\kappa \equiv \Gamma(\kappa + 1)/[\Gamma(\kappa - 1/2)(\kappa - 3/2)^{3/2}]$ is a normalization constant. This kappa distribution is plotted in Figure 1 for various values of the parameter κ; note that for $E \gg (\kappa - 3/2)kT$ the distribution declines with energy as a power law of index $\kappa + 1$, whereas for $E \lesssim (\kappa - 3/2)kT$ the number of particles can be closely fit by a Maxwellian distribution. We can characterize this subpopulation of low-energy core particles by the most-probably-speed energy, E_p, defined by

$$\frac{\partial}{\partial E}(fE)|_{E=E_p} \equiv 0,$$

which yields in a kappa distribution,

$$\frac{E_p}{kT} = \frac{\kappa - 3/2}{\kappa}. \tag{A3}$$

This ratio represents the ratio of core energy to total energy and so describes the degree to which a given kappa distribution can be approximated by a Maxwellian. In particular, note that for $\kappa \to \infty$, we have $E_p/kT \to 1$—as required for this special limiting case in which a kappa distribution approaches a Maxwellian shape—whereas, for finite $\kappa > 3/2$, we have $0 < E_p/kT < 1$. Together, the temperature T and the energy ratio E_p/kT provide a convenient way to characterize physically the kappa distribution, the first as a parameter of the total energy at unit density and the second as a measure of how nearly the distribution approximates a Maxwellian.

APPENDIX B

CROSS SECTIONS AND RATES

In order to calculate each rate coefficient in an arbitrary electron distribution, we must know the cross section σ as a function of speed v (or kinetic energy $E = mv^2/2$). For direct collisional ionization, the cross section has been given by Lotz (1967) as an approximate function of energy as,

$$\sigma_c(E) = 0, \qquad E \le \chi$$

$$= C_c \frac{\ln(E/\chi)}{E}, \qquad E \ge \chi, \tag{B1a}$$

where χ is the ionization threshold energy and C_c is a dimensional constant. In the total ionization cross section, we

include a correction for autoionization following inner shell excitation,

$$\sigma_a(E) = 0, \qquad E < \chi,$$

$$= \frac{C_a}{E}, \qquad E \geq \chi. \tag{B1b}$$

For direct radiative recombination, we assume the cross section varies as a power law in energy,

$$\sigma_r(E) = \frac{C_r}{E^a}, \tag{B1c}$$

where C_r is again a constant and a is the power law index for which typically $1/2 < a < 1$ (see, e.g., Osterbrock 1974). In contrast, because dielectronic recombination is a resonant process involving bound states at discrete energies E_i, we write

$$\sigma_d(E) = \sum_i C_i \delta(E - E_i), \tag{B1d}$$

where, in principle, the sum is taken over many hundreds of bound states, but in practice we include here only the two most dominant terms.

Performing the integral in equation (2) for rates in a Maxwell-Boltzmann distribution at a temperature T (eq. [A1]), we obtain the rate coefficients

$$\langle \sigma_c v \rangle_{\max} = \left[4C_c(2\pi mkT)^{-1/2}\right] E_1(\chi/kT) \tag{B2a}$$

$$\langle \sigma_a v \rangle_{\max} = \left[4C_a(2\pi mkT)^{-1/2}\right] \exp(-\chi/kT) \tag{B2b}$$

$$\langle \sigma_r v \rangle_{\max} = \left[4C_r(2\pi mkT)^{-1/2}\right] \frac{\Gamma(2-a)}{(kT)^{a-1}} \tag{B2c}$$

$$\langle \sigma_d v \rangle_{\max} = \left[4(2\pi mkT)^{-1/2}\right] \sum_i C_{di} \frac{E_i}{kT} \exp(-E_i/kT), \tag{B2d}$$

where E_1 is the first exponential integral (Abramowitz and Stegun 1972), and Γ is again the factorial function. The constants in these expressions can be evaluated by comparing equations (B2) with the analytic rate functions given by Lotz (1967), Aldrovandi and Péquignot (1973, 1976), Sarazin (1979), and Shull and Van Steenberg (1982); the values used here are summarized in Table 1. For a given ionization balance, the Maxwellian rate coefficients depend on only the temperature T.

The analogous rates in a kappa distribution given by equation (A2) are of the form

$$\langle \sigma_c v \rangle_\kappa = \left[4C_c(2\pi mkT)^{-1/2}\right] A_\kappa \frac{{}_1F_2(\kappa, \kappa; \kappa+1; -(\kappa-3/2)kT/\chi)}{\kappa^2/(\kappa-3/2)} [(\kappa-3/2)kT/\chi]^\kappa, \tag{B3a}$$

$$\langle \sigma_a v \rangle_\kappa = \left[4C_a(2\pi mkT)^{-1/2}\right] A_\kappa (\kappa-3/2)/\kappa \Big/ \left[1 + \frac{1}{(\kappa-3/2)} \frac{\chi}{kT}\right]^\kappa, \tag{B3b}$$

$$\langle \sigma_r v \rangle_\kappa = \left[4C_r(2\pi mkT)^{-1/2}\right] \frac{\Gamma(2-a)}{(kT)^{a-1}} \frac{\Gamma(\kappa+a-1)}{\Gamma(\kappa-1/2)(\kappa-3/2)^{a-1/2}}, \tag{B3c}$$

$$\langle \sigma_d v \rangle_\kappa = \left[4(2\pi mkT)^{-1/2}\right] \sum_i C_{di} \frac{E_{di}}{kT} A_k \Big/ \left[1 + \frac{1}{\kappa-3/2} \frac{E_i}{kT}\right]^{\kappa+1}, \tag{B3d}$$

where A_κ is a normalization constant (Appendix A), and the Gauss hypergeometric function ${}_1F_2$ (Abramowitz and Stegun 1972) is most easily evaluated for integer kappa as a finite series obtained through repeated integration by parts

TABLE 1

ASSUMED VALUES FOR RATE CONSTANTS[a]

Ion	C_c	C_a	C_r	C_{d1}	C_{d2}	a	χ	E_{d1}	E_{d2}
O^{+6}	1.7(−28)	0	1.0(−33)	2.0(−30)	3.3(−31)	1.24	739	603	715
Fe^{+11} ...	6.1(−28)	3.1(−29)	6.9(−33)	5.8(−29)	1.6(−29)	1.20	331	52.6	155

[a]Energies in eV; rate constants in CGS units.

of the integral in equation (2) (Gradshteyn and Ryzhik 1979, eq. [2.111.3], p. 58). As in the Maxwellian case, the rate coefficients in a kappa distribution depend on the temperature T, but, in addition, they also depend on the distribution shape, as set by the free parameter κ. Note that as $\kappa \to \infty$, the rates in equations (B3) approach the Maxwellian forms (B2), as required.

REFERENCES

Abramowitz, M., and Stegun, I. A. 1972, *Handbook of Mathematical Functions* (Washington: Government Printing Office).
Aldrovandi, S. M. W., and Péquignot, D. 1973, *Astr. Ap.*, **25**, 137.
_____. 1976, *Astr. Ap.*, **47**, 321.
Allen, J. W., and Dupree, A. K. 1969, *Ap. J.*, **155**, 27.
Bame, S. J., Asbridge, J. R., Feldman, W. C., and Kearney, P. D. 1974, *Solar Phys.*, **35**, 137.
Bame, S. J., Hundhausen, A. J., Asbridge, J. R., and Strong, I. B. 1968, *Phys. Rev. Letters*, **20**, 393.
Belcher, J. W., Goertz, C. W., and Bridge, H. S. 1980, *Geophys. Res. Letters*, **7**, 17.
Billings, D. E. 1966, *A Guide to the Solar Corona* (New York: Academic Press).
Bridge, H. S., *et al.* 1974, *Science*, **185**, 4131.
Burgess, A. 1965, *Ap. J.* (*Letters*), **141**, 1588.
Feldman, W. C., Asbridge, J. R., Bame, S. J., Montgomery, M. D., and Gary, S. P. 1975, *J. Geophys. Res.*, **80**, 4181.
Fenimore, E. E. 1980, *Ap. J.*, **235**, 245.
Garret, H. B. 1979, *Rev. Geophys. Space Phys.*, **17**, 397.
Gradshteyn, I. S., and Ryzhik, I. M. 1979, *Table of Integrals, Series, and Products* (New York: Academic Press).
Hundhausen, A. J. 1977, in *Coronal Holes and High Speed Wind Streams*, ed. J. B. Zirker (Boulder: Colorado Associated University Press), p. 225.
Hundhausen, A. J., Gilbert, H. E., and Bame S. J. 1968*a*, *Ap. J.* (*Letters*), **152**, L3.
_____. 1968b, *J. Geophys. Res.*, **73**, 5485.
Jacobs, B. L., Davis, J., Kepple, K. C., and Blaha, M. 1977, *Ap. J.*, **211**, 605.
Jordan, C. 1969, *M.N.R.A.S.*, **142**, 501.
_____. 1970, *M.N.R.A.S.*, **148**, 17.
Kraus, J. D. 1966, *Radio Astronomy* (New York: McGraw-Hill).
Krimigis, S. M., Carbary, J. F., Keath, E. P., Bostrom, C. O., Axford, W. I., Gloeckler, G., Lanzerotti, L. J., and Armstrong, T. P. 1981, *J. Geophys. Res.*, **86**, 8227.
Leer, E., and Holzer, T. E. 1979, *Solar Phys.*, **63**, 143.
Lotz, W. 1967, *Ap. J. Suppl.*, **14**, 207.
Montgomery, M. D. 1972, in *Cosmic Plasma, Physics*, ed. K. Schindler (New York: Plenum Press), p. 61.
Montgomery, M. D., Bame, S. J., and Hundhausen, A. J. 1968, *J. Geophys. Res.*, **73**, 4999.
Munro, R. H., and Jackson, B. V. 1977, *Ap. J.*, **213**, 874.
Ogilvie, K. W., and Scudder, J. D. 1978, *J. Geophys. Res.*, **83**, 3776.
Ogilvie, K. W., *et al.* 1974, *Science*, **185**, 4146.
Ogilvie, K. W., Scudder, J. D., Vasyliunas, V. M., Hartle, R. E., and Siscoe, G. L. 1977, *J. Geophys. Res.*, **82**, 1807.
Ogilvie, K. W., and Vogt, C. 1980, *Geophys. Res. Letters*, **7**, 577.
Olbert, S. 1969, in *Physics of Magnetospheres*, ed. R. C. Carovillano, J. F. McClay, and H. R. Radoski, (Dordrecht: Reidel), p. 641.
Olbert, S., Egidi, A., Moreno, G., and Pai, L. G. 1967, *Trans. AGU*, **48**, 177.
Osterbrock, D. E. 1974, *Astrophysics of Gaseous Nebulae* (San Francisco: W. H. Freeman).
Owocki, S. P. 1982, Ph.D. thesis, University of Colorado; NCAR CT-66, Boulder.
Owocki, S. P., and Scudder, J. D. 1982, in *Second Cambridge Conference on Cool Stars*, ed. M. Giampappa and L. Golub, *SAO Spec. Rept. 392*, Vol. **1**, p. 107.
Rosenbauer, H., Miggemeider, H., Montgomery, M. and Schwenn, R. 1976, in *Physics of Solar and Planetary Environments*, ed. D. Williams (Washington: American Geophysical Union), p. 319.
Roussel-Dupré, R. 1979, Ph.D. thesis, University of Colorado, Boulder.
_____. 1980*a*, *Solar Phys.*, **68**, 243.
_____. 1980*b*, *Solar Phys.*, **68**, 265.
Sarazin, C. L. 1979, private communication.
Scudder, J. D. and Olbert, S. 1979*a*, *J. Geophys. Res.*, **84**, 2755.
_____. 1979b, *J. Geophys. Res.*, **84**, 6603.
_____. 1983, in preparation.
Scudder, J. D., Sittler, E. C., Jr., and Bridge, H. S. 1981, *J. Geophys. Res.*, **86**, 8157.
Seaton, M. J. 1964, *Planet. Space Sci.*, **12**, 55.
Shoub, E. C. 1983, *Ap. J.*, **266**, 339.
Shull, J. M., and Van Steenberg, M. 1982, *Ap. J. Suppl.*, **48**, 95.
Sittler, E. C., Jr., Scudder, J. D., and Bridge, H. S. 1981, *Nature*, **292**, 711.
Smerd, S. F. 1964, in *AAS-NASA Symposium on Solar Flares*, NASA SP-50.
Strobel, D. F., and Davis, J. 1980, *Ap. J.* (*Letters*), **238**, L49.
Vasyliunas, V. M. 1968, *J. Geophys. Res.*, **73**, 2866.
Wilson, D. C. 1977, Ph. D. thesis, University of Colorado; NCAR CT-40, Boulder.

S. P. OWOCKI: Center for Astrophysics, 60 Garden Street, Cambridge, MA 02138

J. D. SCUDDER: NASA Goddard Spaceflight Center, Laboratory for Extraterrestrial Physics, Greenbelt, MD 20771